Neuron, Volume *109*

Supplemental information

A mechanism for inter-areal coherence through communication based on connectivity and oscillatory power

Marius Schneider, Ana Clara Broggini, Benjamin Dann, Athanasia Tzanou, Cem Uran, Swathi Sheshadri, Hansjörg Scherberger, and Martin Vinck

Supplementary Figures to: A mechanism for inter-areal coherence through communication based on connectivity and oscillatory power

Marius Schneider[a,d,f], Ana Clara Broggini[a], Benjamin Dann[b], Athanasia Tzanou[a], Cem Uran[a], Swathi Sheshadri[b,c], Hansjörg Scherberger[b,c], Martin Vinck[a,d,e,f]

[a] *Ernst Strüngmann Institute (ESI) for Neuroscience in Cooperation with Max Planck Society, 60528 Frankfurt am Main, Germany*
[b] *German Primate Center, 37077 Göttingen, Germany*
[c] *Faculty of Biology and Psychology, University of Goettingen, 37073 Goettingen, Germany*
[d] *Donders Centre for Neuroscience, Department of Neuroinformatics, Radboud University Nijmegen, 6525 Nijmegen, Netherlands*
[e] *Lead contact*
[f] *Correspondence: marius.schneider@esi-frankfurt.de (M.S.), martin.vinck@esi-frankfurt.de (M.V.)*

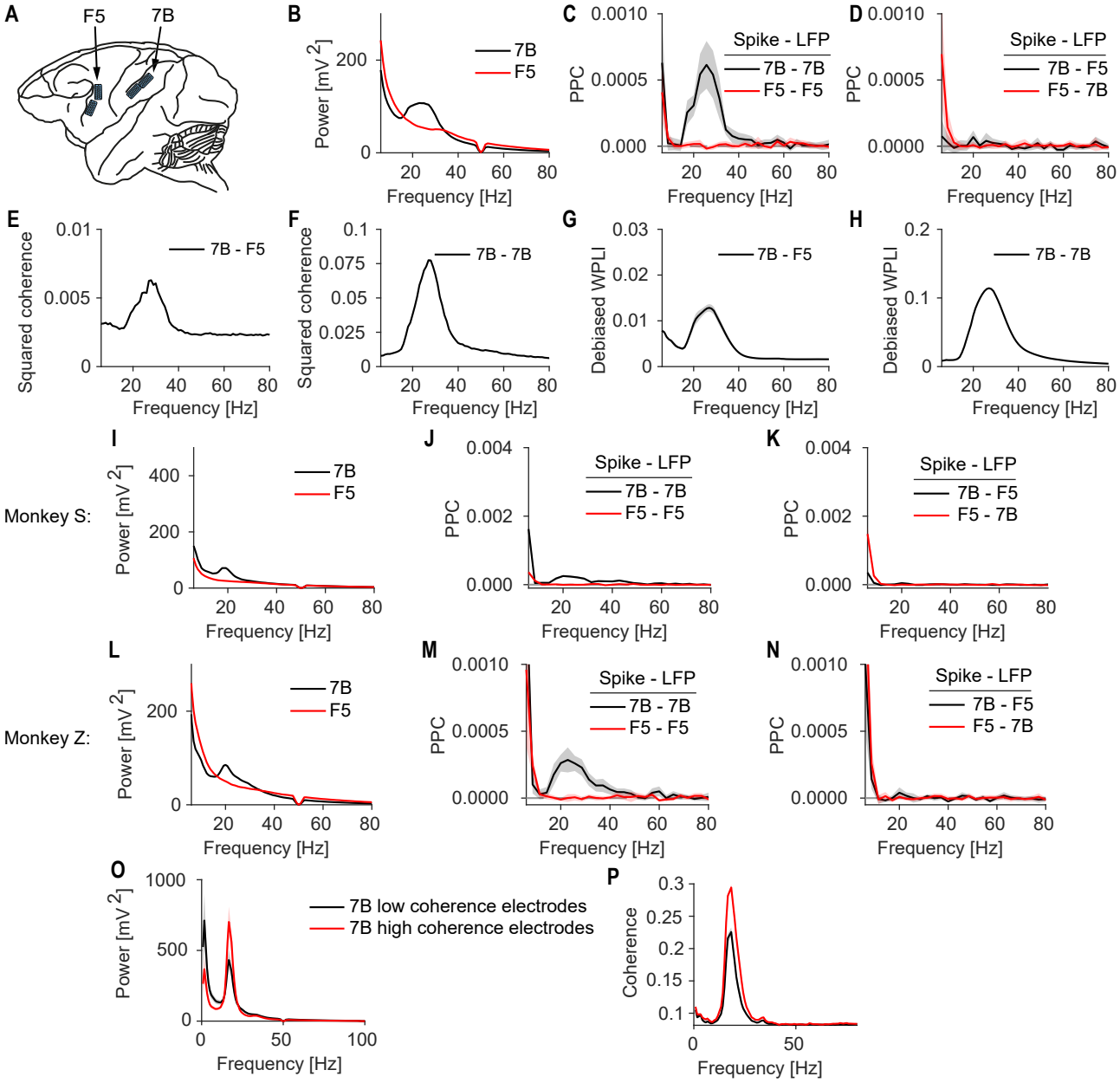

Figure S1: Beta coherence between 7B and F5 for both monkeys and during the movement period. Related to Figure 1.
(A-H) Same as Figure 1, but for Monkey Z. **(I-N)** Power spectra and spike-field locking in the movement period, for both monkeys. Same naming conventions as in Figure 1. **(O)** Power of 50% of the electrodes in 7B that have a high (red)/low(black) coherence with area F5 (Monkey S). **(P)** Coherence between of 50% of the electrodes in 7B that have a highest (red)/lowest(black) coherence with area F5. Coherence is averaged across all electrodes of Area F5 (Monkey S).

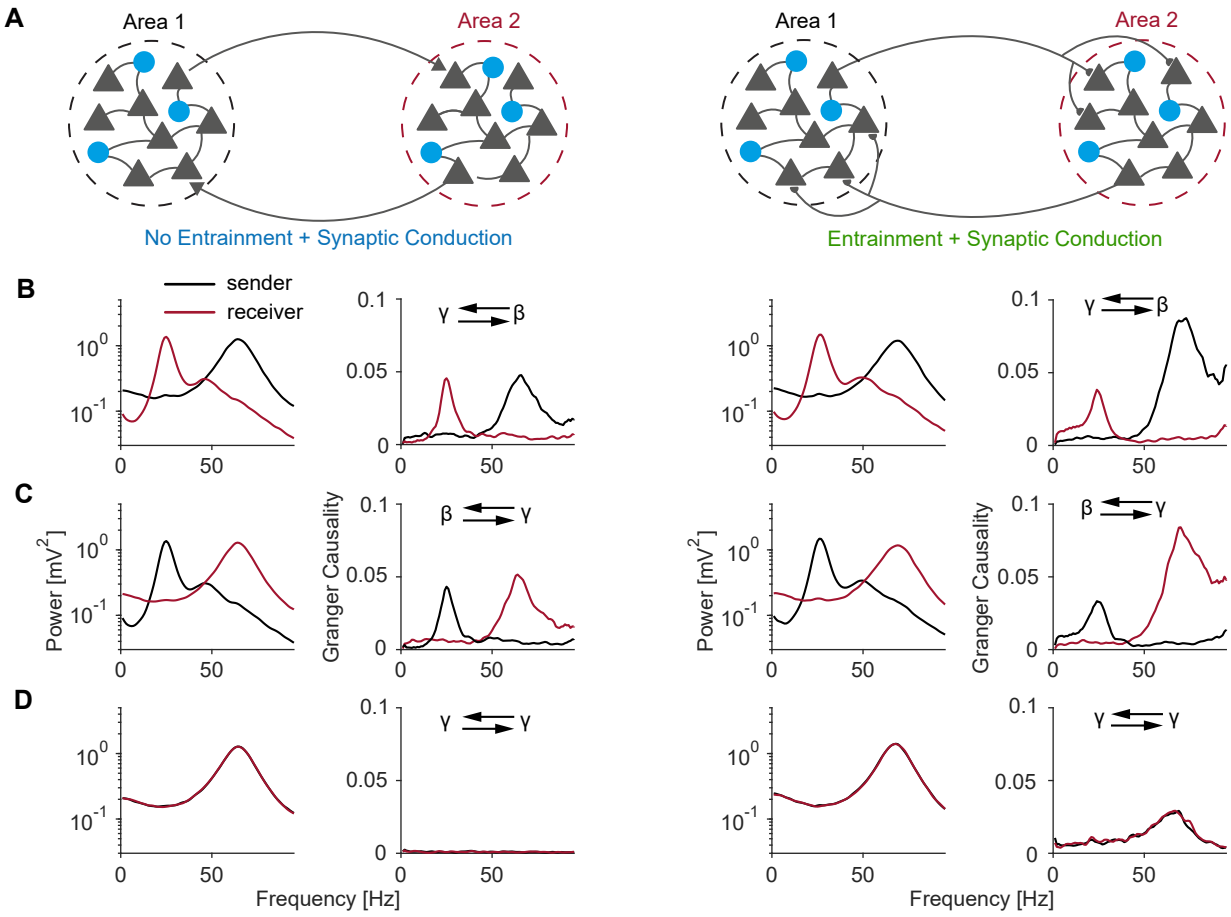

Figure S2: Granger-causality in bidirectionally coupled E/I network. Related to Figure 3 and 8.
(A) Illustration of the two models. Each area consisted of a population of spiking neurons whose dynamics were modeled by stochastic Wilson-Cowan equations. In the first model (left two columns), synaptic potentials due to inputs from Area-1 were superimposed onto the synaptic potentials from Area-2 itself and vice versa. Neurons in Area-2/Area-1 were "blind" to the synaptic inputs from Area-1/Area-2, i.e. spiking entrainment was prohibited. The second model (right two columns) is identical to the first model, however, synaptic inputs from Area-1/Area-2 could now entrain the neurons in Area-2/Area-1. **(B)** First two columns: Area 1 oscillates at gamma and Area 2 at beta. Spectral Granger causality shows clear peaks, following the power in the sender. Last two columns: Spiking entrainment increases Granger influences slightly. **(C)** and **(D)** Same as in (B), but now with different oscillation frequencies. When the oscillation frequency in the sender matches with the receiver, there is an increase in LFP-LFP Granger influence due to spiking (D). (B-D) all for coupling value of $w = 0.1$.

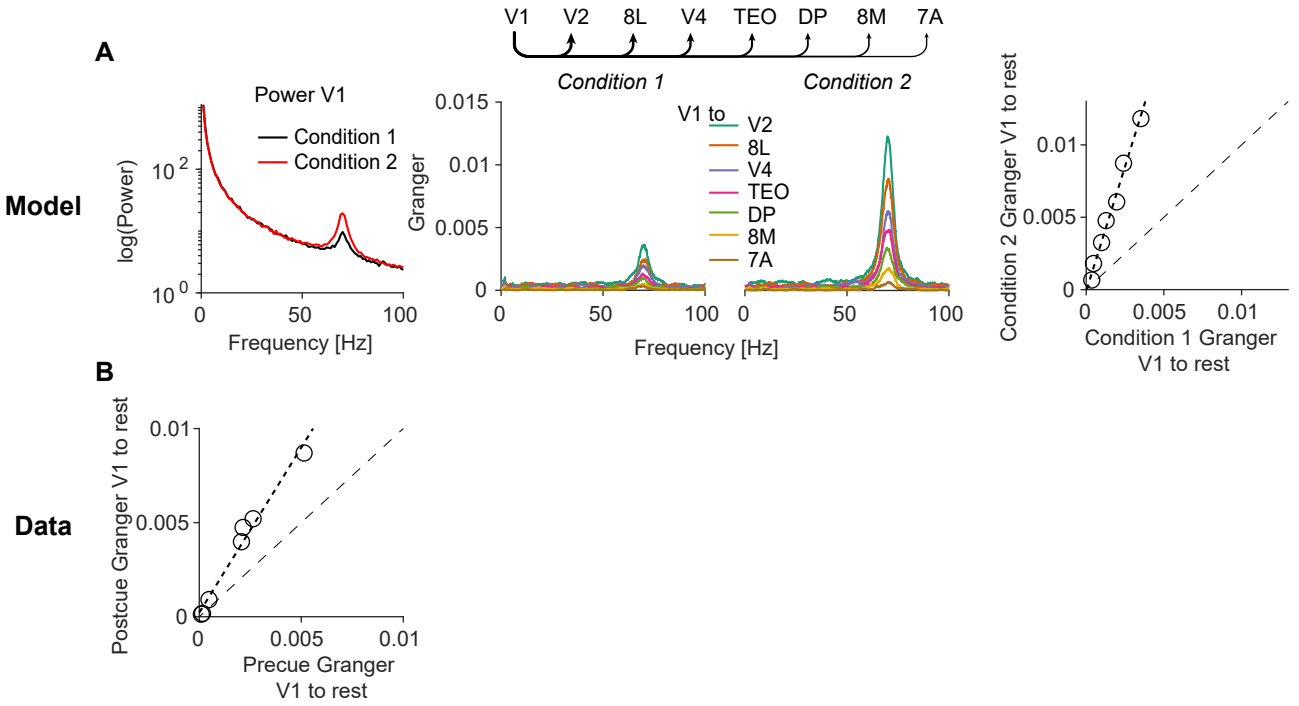

Figure S3: Modelling changes in Granger-causality between V1 and higher areas with attention. Related to Figure 3.
(A) Simulated inter-areal interactions between a sender area that shows gamma oscillations of different strength in two conditions and 7 receiver areas with different connection weights. Power spectra with gamma oscillations of different strength (left), granger influence from V1 to the the other areas in condition one (center-left) and condition two (center-right). Granger causality peaks between V1 and the rest in condition 1 versus condition 2 (right). The parameters were: $\gamma = 0.95, w_{12} = 0.8, w_{12} = 0.7, w_{12} = 0.6, w_{12} = 0.05, w_{12} = 0.04, w_{12} = 0.03, w_{12} = 0.02$ (see Methods: Simulations of SSM model with source-projection coherence). **(B)** Data were extracted from the supplementary figures in Bastos et al. (2015) using Adobe Illustrator on the vector graphics. We hypothesized that if gamma feedforward Granger-influences from V1 to other higher areas are driven by the presence of a strong gamma source, then they should change by approximately the same factor if V1 gamma power increases. It is known that V1 gamma power increases after the presentation of an attentional cue (post-cue) as compared to the pre-cue period (Richter et al., 2019; Bosman et al., 2012) (unfortunately Bastos et al. (2015) did not publish power spectra for different conditions or for different areas). Each data point represents the gamma Granger-causality from V1 to higher areas, separately for the pre-cue and post-cue condition. Consistent with the SSM model predictions, we found that the gamma Granger-influences from V1 to higher areas were increased by approximately the same factor across all areas (1.76; Pearson's R = 0.99).

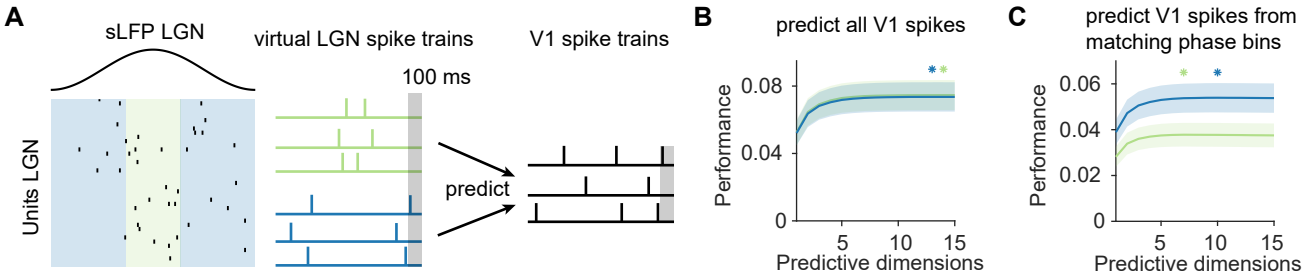

Figure S4: Gamma-phase dependent prediction of V1 activity from LGN firing rates. Related to Figure 5.
(A) LGN spike trains were split into two "virtual" sets of spike trains based on the gamma phase of the sLFP signal in LGN. As in Womelsdorf et al. (2012), phase bins differed in length such that the total number of spikes in the LGN remained the same for the two phase bins. Virtual LGN spike train activity with spikes occurring at different gamma phases was used to predict V1 firing. Predictions were carried out using reduced-rank regression (Semedo et al., 2019). Spike counts were taken in 100ms bins. **(B)** V1 firing rates were predicted without binning V1 spikes into phase-dependent bins. Predictive performance of virtual spike trains in LGN at maximally excitable (green) and less excitable (blue) gamma phase using reduced rank regression. Asterisks indicate the minimum number of predictive dimensions with full performance. Prediction of V1 firing rates by LGN firing rates did not differ between the sets of spikes occurring during excitable and non-excitable gamma phases. **(C)** Same as (B) but instead of predicting all spikes of the population in V1, V1 activity was predicted after binning V1 spikes according to gamma phase. The excitable gamma phase bin was shifted 3ms forward in time compared to the LGN, in order to account for the LGN-V1 transmission delay.

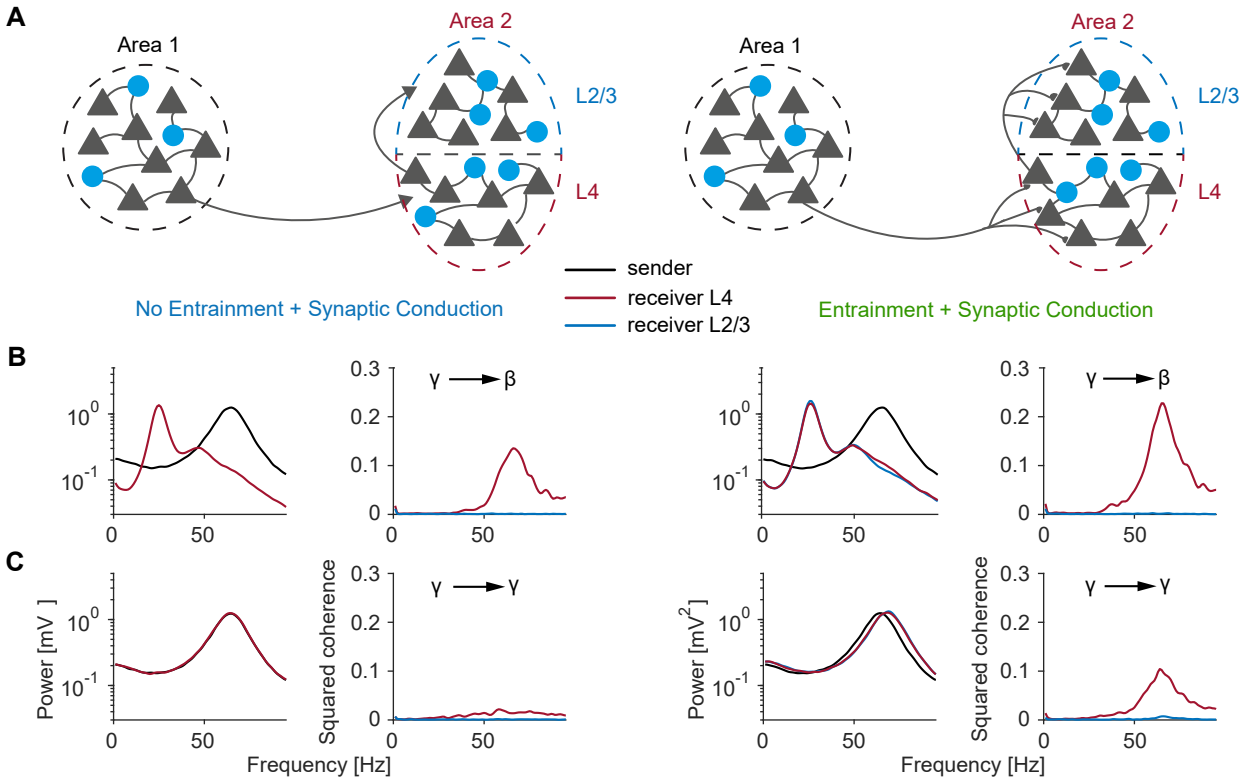

Figure S5: Coherence between a sender and a receiver consisting of two laminar compartments. Related to Figure 8.
(A) Illustration of the two models. Area 1 consisted of a population of spiking neurons whose dynamics were modeled by stochastic Wilson-Cowan equations. Area 2 was divided into a granular layer (L4) and a superficial layer (L2/3). Each layer consisted of a population of spiking neurons whose dynamics were modeled by stochastic Wilson-Cowan equations. In the first model (left two columns), synaptic potentials due to inputs from Area 1 were superimposed onto the synaptic potentials from L4 of Area 2 itself. In the same way, synaptic potentials due to inputs from Area 2 L4 were superimposed onto the synaptic potentials from L2/3 of Area 2 itself. Neurons in L4 of Area 2 were "blind" to the synaptic inputs from Area 1, i.e. spiking entrainment was prohibited. Neurons in L2/3 of Area 2 were "blind" to the synaptic inputs from Area 2 L4. The second model (right two columns) is identical to the first model, however synaptic inputs from Area-1 and Area-2 L4 could now entrain the neurons in L4 of Area-2 and L2/3 of Area-2. **(B)** First two columns: Area 1 oscillates at gamma and the two layers of Area 2 at beta. Coherence spectra show clear peaks, following the power in the sender. Last two columns: Spiking entrainment increases coherence slightly. **(C)** Same as in (B), but now with different oscillation frequencies. When the oscillation frequency in the sender matches with the receiver, there is an increase in LFP-LFP coherence due to spiking. (B-C) all for a coupling value of $w = 0.1$. The two layers of Area-2 always oscillate at the same frequency.

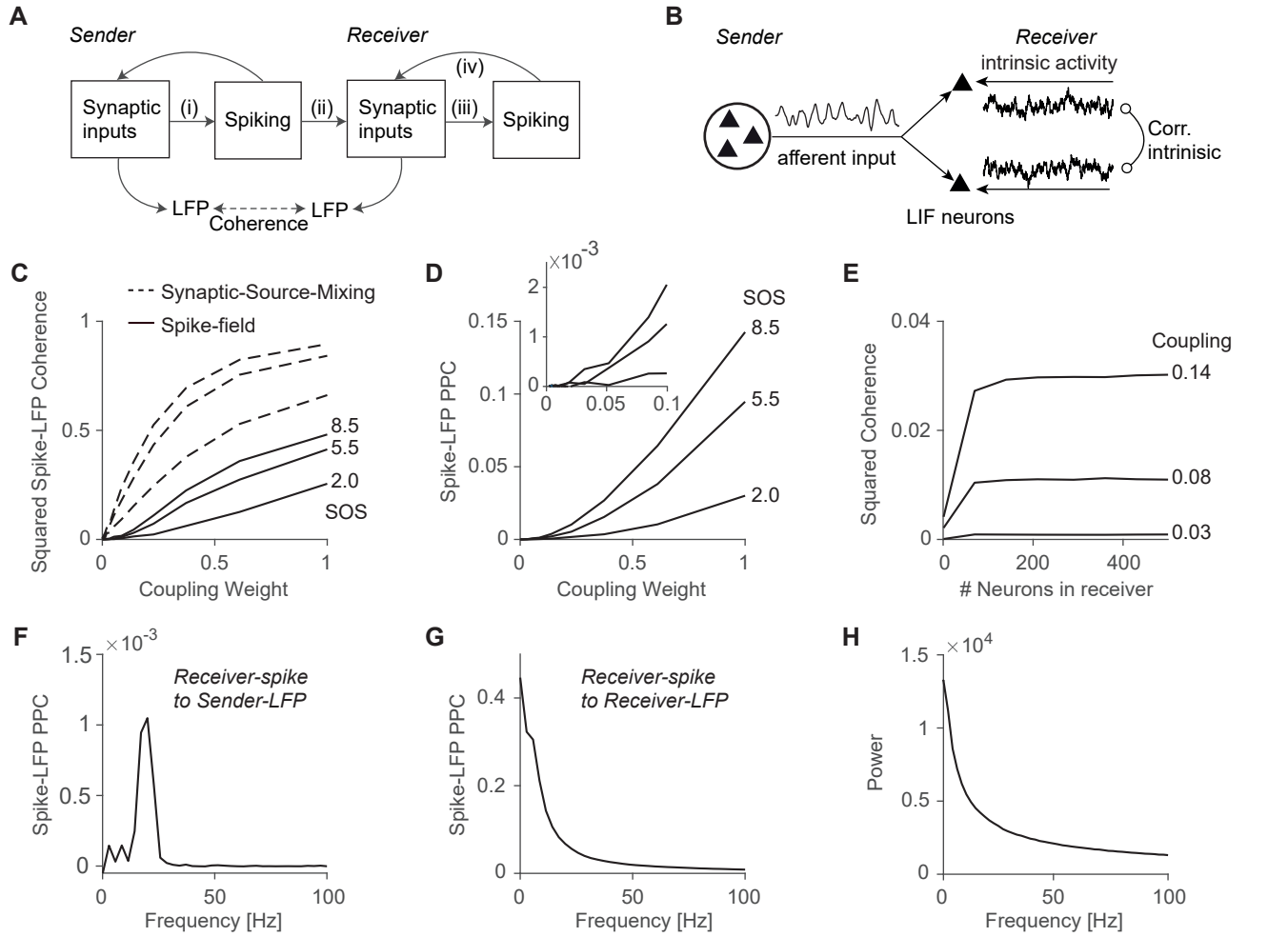

Figure S6: Coherence between sender and receiver's spiking activity for LIF neurons. Related to Figure 8.
(A) Illustration of the different mechanisms contributing to inter-areal LFP coherence. Spiking activity in the sender (i) causes afferent synaptic inputs in the receiver. These inputs may not be a coherent copy of the LFP signal in Area-1 (source-projection coherence). Synaptic inputs in the receiver give rise to additional spiking activity (iii), which through recurrent connections will give rise to synaptic inputs in the receiver (iv). In the case of resonance, oscillatory inputs may be amplified through recurrent dynamics at (iii) and (iv). The LFP, in the typical frequency range ($< 80Hz$), is a proxy of the population synaptic activity. **(B)** Illustration of model simulations on spike phase-locking. The receiving area is modeled as a population of leaky integrate-and-fire (LIF) neurons, whose intracellular potentials are a mixture of oscillatory input from sending Area-1 and intrinsic $1/f$ fluctuations in the receiver. The local fluctuations are correlated to different degrees. In the panels below, we use a correlation value of 0.5. We summed the spikes across all neurons to construct the summed population activity and then computed the coherence with the sender LFP. **(C)** Squared coherence between summed population spiking activity in the receiver and the sender LFP, for different values of SOS and coupling weight (solid lines). LFP-LFP coherence due to afferent synaptic inputs corresponds to dashed lines. Note similar dependences between LFP-spike and LFP-LFP coherence on SOS and coupling weight. However, there was higher LFP-LFP coherence between the sender and the afferent synaptic inputs, than between the sender and the population spiking activity in the receiver. One reason for this difference is that non-linear input-output transformations introduce a distortion in the coherence, and introduce interactions across frequencies to which coherence (being a linear measure) is blind. Another reason is that the outputs of individual neurons are stochastic and sparse. Hence, spikes cannot encode afferent synaptic inputs without distortion. Distortion will be greater for a small number of neurons in the receiver as shown in (C). **(D)** Spike-field phase-locking (unbiased PPC) between individual neurons in the receiver population and the LFP signal in the sender. Spike-field PPC shows similar dependencies on SOS and connectivity as spike-field coherence. Note relatively small spike-field PPC values for realistic connectivity weights around 0-0.1. (These PPC values are consistent with the empirical data observed in Figure 1, 5). **(E)** The number of neurons in the receiver determines the spike-LFP coherence. Inter-areal coherence between Area-1 LFP and Area-2 spikes increases with the number of receiver neurons. This is expected, because a larger number of neurons will provide a better sampling of the input rhythm, as each neuron fires sparsely and with random variation. For enough neurons, an asymptote is reached (which is shown in (C)). In this simulation, the SOS at the oscillatory frequency $f_1 = 20Hz$ was $SOS(f_1) = 5.5$ **(F)** The Spectrum of spike-field PPC of receiver spikes of individual neurons to sender LFP. There is a clear beta-peak in the inter-areal spike-LFP PPC. **(G)** Spike-field PPC of receiver spikes to the receiver LFP. There is no beta-peak in the spike-LFP PPC in the receiver, consistent with the absence of intrinsic oscillations in the receiver. **(H)** Power spectrum of the receiver LFP. Despite the afferent oscillatory input, the population spiking activity does not show a peak at the sender oscillation frequency (beta). Instead, the spectrum follows the 1/f activity of the local fluctuations. Together with (G) and (H), this shows that rhythmicity in afferent inputs effectively disappears in the receiver, both at the synaptic and the spiking level. (F-H) The parameters were: $SOS = 5.5$, $w = 0.08$.

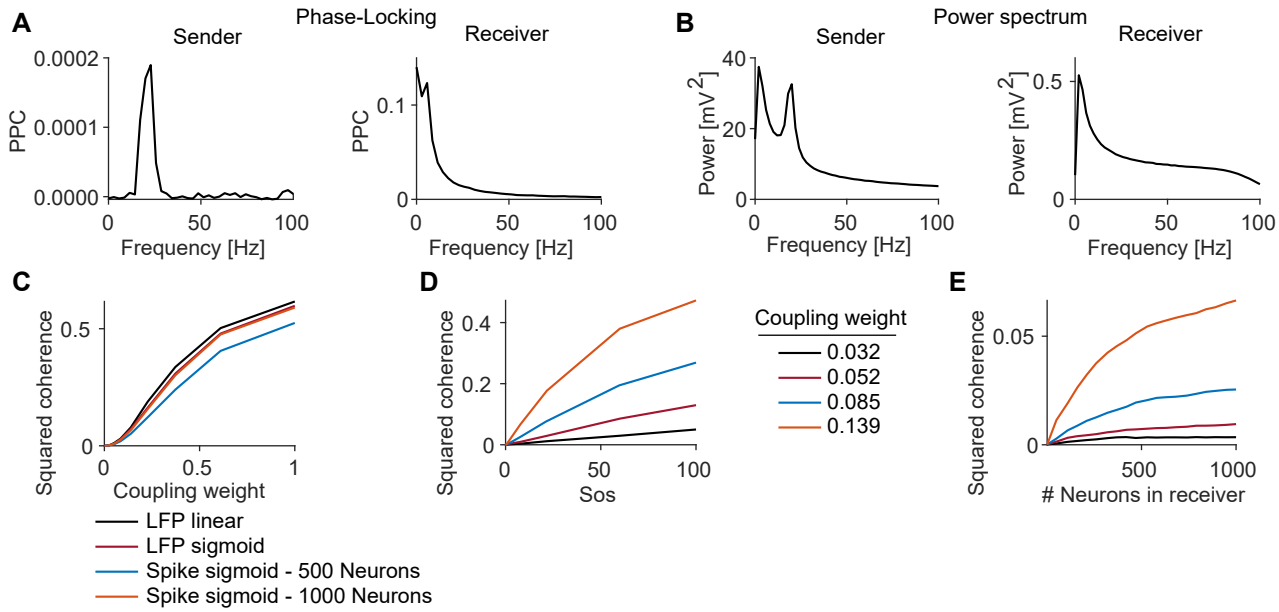

Figure S7: Coherence between sender and a receiver's spiking activity for neurons with a sigmoidal input-output relationship. Related to Figure 8. The receiver was modeled as a population of 1000 neurons modulated by the synthetic LFP signal as in (Figure 3B) according to an inhomogeneous Poisson process. **(A)** Phase-locking of individual neurons to the sender (left) and receiver (right) LFP. The phase-locking to the sender LFP signal shows a narrow-band peak at the modulation frequency. **(B)** Power spectra of both areas. The sender area follows the power spectrum expected from the model in Figure 3B. The power spectrum of the summed activity of neurons in the receiver area does not show a peak at the frequency of the transmitted oscillatory signal. **(C)** For a high number of neurons, the coherence between sender LFP and receiver LFP approaches the LFP-LFP coherence that is predicted from synaptic inputs. The LFP-LFP coherence (black) is generated with the Synaptic-Source-Mixing model from Figure 3B. In addition, we have generated an LFP-LFP model where the receiver signal depends sigmoidally on the transmitter signal. As predicted, coherence is comparable between the linear and sigmoidal cases. As the number of neurons increases, the coherence between sender LFP and population spiking output approaches the LFP-LFP coherence due to afferent synaptic inputs. **(D)** The inter-areal coherence through sigmoidally modulated input-output relation of spiking shows similar dependencies on coupling and SOS similar to synaptic mixing. **(E)** Inter-areal coherence increases with the number of entrained neurons in the receiver. Depending on the coupling weight and the SOS the squared coherence saturates at a certain number of neurons.

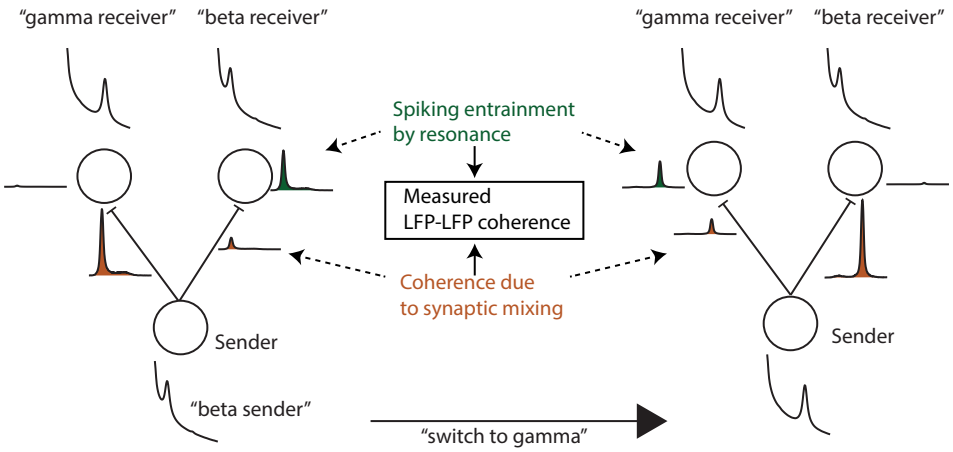

Figure S8: Illustration of the difference between LFP-LFP coherence and spiking entrainment, and ability to switch communication by changing oscillations in the sender. Related to Figure 8.
In the left case, the sender oscillates at beta, and it would have a high LFP-LFP coherence with a receiver at gamma due to synaptic mixing. However, this LFP coherence does not translate into spiking entrainment. When the receiver also oscillates at beta, the LFP coherence due to synaptic mixing is lower, but due to resonance, the receiver will now exhibit more spiking entrainment. In the right case, the sender switches to gamma and now switches communication to the gamma receiver. Paradoxically, LFP-LFP coherence might be higher between the sender and the receiver that communicate less.